Excitation functions of He($n=3$) levels in the intermediate-velocity regime of He^+-He collisions

R. Okasaka, K. Kawabe, S. Kawamoto, M. Tani, H. Kuma, T. Iwai, K. Mita, and A. Iwamae
Department of Engineering Science, Kyoto University, Kyoto 606-01, Japan
(Received 8 February 1993)

We measured cross sections of target He atoms (σ_T) and those of electron capture into the excited levels of projectile ions (σ_P) for He $3^{1,3}S,P,D$ levels in He^+-He symmetric collisions in the energy range 20–300 keV. By phenomenological analysis of the excitation functions, we found structures characteristic of the intermediate-velocity regime for both σ_T and σ_P: the magnitudes and the velocities of the peak positions of the structures show notable dependence on the angular-momentum states of the levels. Similar dependence on angular-momentum states is also recognized in the excitation functions for electron capture by protons into H($3,l$) levels in H^+-Li and H^+-He collisions obtained by other investigators. This fact suggests close correlation between the behaviors of the excitation functions and the angular-momentum states of the initial and the final states, because all the processes mentioned above are concerned with electron transfer from the s level to upper s, p, and d levels. A simple momentum-matching electron-transfer model explains the observed characteristics qualitatively. Characteristics observed for the structures of σ_P are also observed for the structures of σ_T, although the structure of σ_P appears in a velocity range about 1.4 times larger than that for the structure of σ_T. Thus we expect that the same kind of mechanism that governs electron capture into excited states also causes target excitation accompanied by electron exchange.

PACS number(s): 34.70.+e

I. INTRODUCTION

On studies of mechanisms of excitation in ion-atom collisions, the high-velocity (energy) regime of an excitation function is defined as the velocity range where relative velocity of colliding particles v(rel) is much larger than classical orbital velocities of bound electrons v(elec):

$$v(\text{rel}) \gg v(\text{elec}) . \tag{1}$$

In this velocity regime the Born approximation of the first-order-perturbation method well describes behaviors of cross sections of excitation and ionization of target atoms as a function of collision velocity.

The low-velocity (energy) regime is defined as

$$v(\text{rel}) \ll v(\text{elec}) . \tag{2}$$

The mechanism of molecular excitation through quasimolecular states formed during the collisional interaction is dominant in this velocity regime, while the multichannel close-coupling method successfully explains behaviors of the excitation cross section of the target atom and of the cross section of electron capture into an excited state by projectile.

The velocity range between the high- and low-velocity regimes where collision velocities are comparable to electron orbital velocities is usually considered the intermediate-velocity (energy) regime:

$$v(\text{rel}) \sim v(\text{elec}) . \tag{3}$$

Each of Eqs. (1) and (2), however, states only the limiting condition of the relation between v(rel) and v(elec), and gives us no information about the boundary of the intermediate-velocity regime. Moreover, in an asymmetric collision system, the electron orbital velocities generally have different values and the definition of Eq. (3) for the intermediate-velocity regime is ambiguous.

The purpose of this paper is to find out the characteristics of behaviors of excitation functions in the intermediate-velocity regime for a symmetric collision system and to analyze them systematically. What type of excitation mechanism can we derive from the observed results in the intermediate-velocity regime? In this study we measure the excitation functions [1] of He($n=3$) levels of process I, σ_T, and process II, σ_P, on He^+-He collisions:

$$\vec{He}^+ + He \rightarrow \vec{He}^+ + He^*, \quad \text{process I} , \tag{4}$$

$$\vec{He}^+ + He \rightarrow \vec{He}^* + He^+, \quad \text{process II} , \tag{5}$$

where arrows specify incident particles. Asterisks indicate that the particles are in excited levels. In Sec. III A, we identify the low-, the intermediate-, and the high-velocity regimes of the excitation functions, based on the phenomenological behavior of the excitation functions. In Sec. III B the characteristics of the excitation functions in the intermediate-velocity regime are discussed. In Sec. III C we show that the characteristics observed on the He^+-He system are also recognized on the excitation functions of protons capturing electrons into H($3,l$) levels on H^+-Li and H^+-He collisions. We try to explain the characteristics observed on the cross sections of both processes of I and II in the intermediate-velocity regime by introducing the model in which an electron is captured directly into excited-state orbit under the condition of momentum matching.

II. EXPERIMENT

The excitation cross sections of He in the energy range 20–300 keV were measured with a 300-keV ion accelerator constructed at the laboratory for the study of plasma physics at the Faculty of Science, Kyoto University. The outline of the experimental setup is shown in Fig. 1. Details of the experimental conditions have been described in Refs. [2] and [3]. The collision cell was a stainless-steel box (50 mm in width, 54 mm in height, 80 mm in length), which has an entrance aperture of 3 mm in diameter at the center of the front wall and an observation aperture of 4 mm on the sidewall. The direction of the observations was set at 45° with respect to the beam direction, in order to separate a Doppler-shifted spectral line emitted by the projectiles from a line emitted by target atoms. A set of optical detecting devices, consisting of a lens of fused silica, a rotatable linear polarizer, a colored-glass filter acting as an order sorter for the observation of the long-wavelength spectral line, a monochromator, and a cooled photomultiplier, measured the intensity of radiation from the region downstream 13 mm from the entrance aperture.

The relation between the cross section σ_i of electron capture into level i and the apparent emission cross section σ_{ij} of the moving projectiles with velocity v is given by Eq. (6) [4],

$$\sigma_i = \frac{\sigma_{ij}}{A_{ij}\tau_i}\left[1-\exp\left[-\frac{l}{\tau_i v}\right]\right]^{-1}, \quad L \ll \tau_i v \ . \tag{6}$$

Here l ($=13$ mm) is the distance from the entrance of the collision cell to the upper stream edge of the observation region, while L is the length of the observation region. In the present experiment, L equals the width of the entrance slit of the monochromator ($=0.1-1$ mm) on which an equal-size image of the beam path in the collision cell is focused and $\tau_i = 1/\sum_{j<i} A_{ij}$ is the mean lifetime of level i.

The total intensity of a spectral-line I in the axial-symmetry collision system is given as $2I_{\parallel}(45°)+I_{\perp}(45°)$ for the observation from the direction of 45° with respect to the beam axis [5], where $I_{\parallel}(45°)$ is the component parallel to the plane containing the beam axis and the observation axis and $I_{\perp}(45°)$ is the component perpendicular to the plane. We define the polarization degree P by the following equations:

$$P = P(90°) = \frac{I_{\parallel}(90°)-I_{\perp}(90°)}{I_{\parallel}(90°)+I_{\perp}(90°)} = \frac{I_{\parallel}(45°)-I_{\perp}(45°)}{I_{\parallel}(45°)} \ , \tag{7}$$

where $P(90°)$ is the polarization obtained in the observation from 90° with respect to the beam axis.

The excitation cross sections of He($n=3$) levels, where n is the principal quantum number, are obtained by the observation of spectral lines in Table I. Figures 2(a)–2(f) show the cross sections of target excitation and electron capture into excited states of the projectile in the velocity range from 1 to 4×10^6 m/sec (about 20–300 keV in He^+-He collisions). The data of Tani, Hishikawa, and Okasaka [3] measured in the energy range 0.5–20 keV were added to our results, and the cross sections of the present experiment were normalized to the values by Tani, Hishikawa, and Okasaka at 20 keV. Statistical uncertainties of the cross sections are as large as twice the size of the data symbols, at most.

The cross sections were not corrected for cascades from the upper levels, for we did not measure upper-level cross sections. We estimated the influence of cascades to ($n=3$)-level cross sections at the collision velocity of 2×10^6 m/s, using the cross sections of $n=4$ and 5 levels in He^+-He collisions obtained from Ref. [4] (Table II). Contributions of cascades are negligible except on P-level cross sections. Cascades to the P level are mainly from upper S levels. They make the magnitude of the P-level cross section large and shift the peak of the excitation function in the intermediate-velocity regime to the high-velocity side, because the peaks of the S-level cross sections appear higher in the velocity range than those of the P-level cross section. Correction for the cascade effect to the P-level cross section does not change the characteristics of excitation functions described by Eqs. (11) and (12) and Eqs. (14) and (15) in Sec. III B, but makes them more significant.

The polarization degrees of emission of $2\,^1P-3\,^1D$ and $2\,^3S-3\,^3P$ transitions are shown in Figs. 3(a) and 3(b). The influence of radiation trapping is serious in the polarization measurement of a 5016-Å line, even in a very-low pressure circumstance [6], and we could not obtain polarization of the 5016-Å line. In order to compare with the collisions of simple-structure projectiles, we measured the excitation cross sections of He atoms in H^+-He collisions.

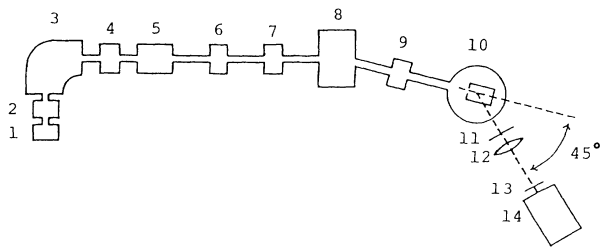

FIG. 1. Experimental apparatus: 1, ion source; 2, Einzel lens and steerer; 3, analyzing magnet; 4, slit; 5, accelerating tube; 6, magnetic q lens; 7, steerer; 8, switching magnet; 9, chopper; 10, collision cell; 11, polarizer; 12, optical lens; 13, filter; 14, monochromator.

TABLE I. The observed spectral lines.

Level	Transition	Target	Projectile 20–300 keV
$3\,^1S$	$2\,^1P-3\,^1S$	7281 Å	7264–7216 Å
$3\,^3S$	$2\,^3P-3\,^3S$	7065 Å	7049–7002 Å
$3\,^1P$	$2\,^1S-3\,^1P$	5016 Å	5004–4971 Å
$3\,^3P$	$2\,^3S-3\,^3P$	3889 Å	3880–3854 Å
$3\,^1D$	$2\,^1P-3\,^1D$	6678 Å	6663–6618 Å
$3\,^3D$	$2\,^3P-3\,^3D$	5876 Å	5862–5824 Å

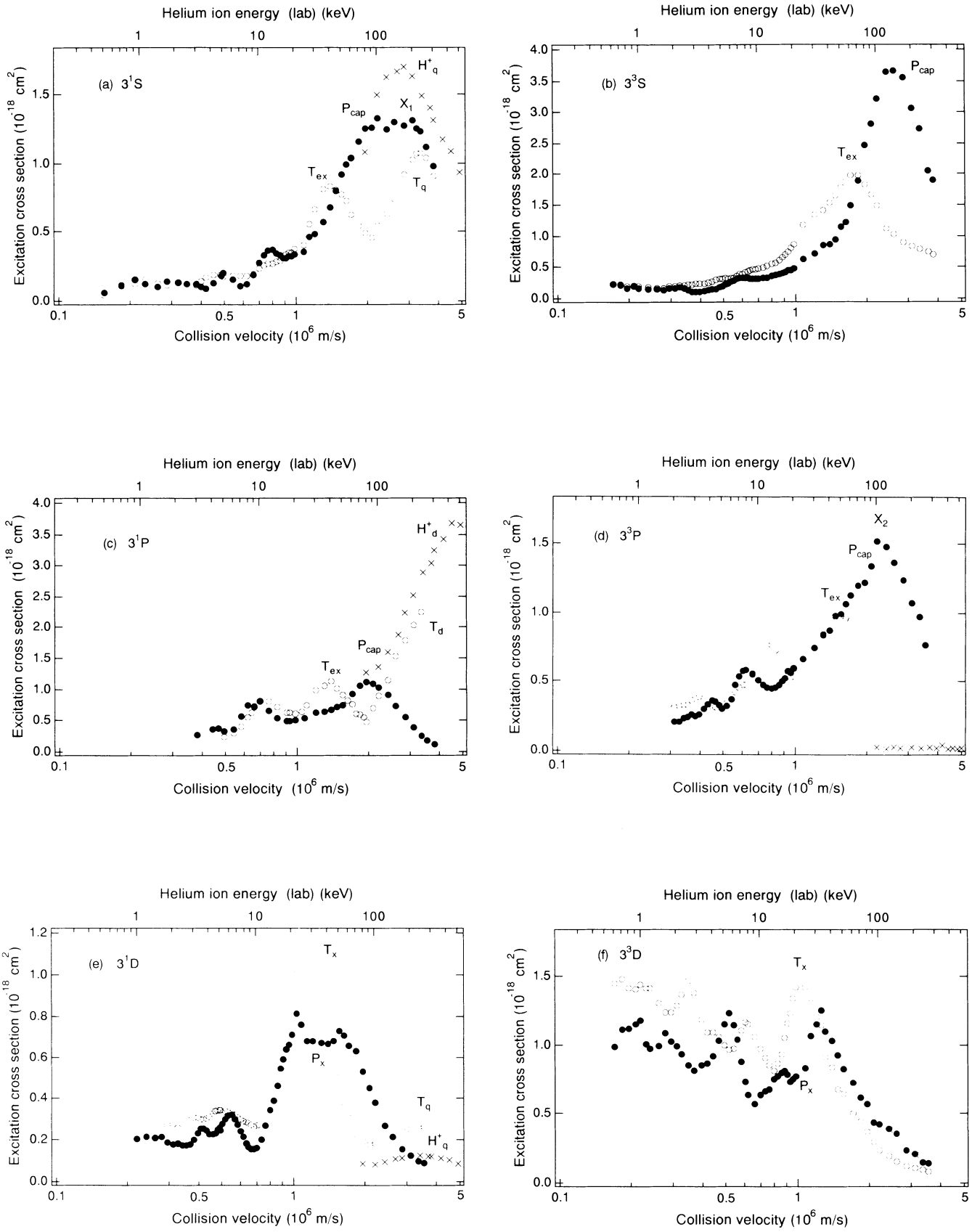

FIG. 2. Excitation functions of He($n=3$) levels. (a) $3\,^1S$, (b) $3\,^3S$, (c) $3\,^1P$, (d) $3\,^3P$, (e) $3\,^1D$, (f) $3\,^3D$. Open circles and solid circles, target excitation (σ_T) and projectile excitation (σ_P) in He^+-He collisions, respectively; crosses, target excitation in H^+-He collisions. See text for symbols.

TABLE II. Contributions of cascade effects from $n=4$ and 5 levels to $n=3$ levels at collision velocity 2×10^6 m/s (%). The excitation cross sections of upper excited levels were obtained from Refs. [4] and [12].

	$3\,^1S$	$3\,^3S$	$3\,^1P$	$3\,^3P$	$3\,^1D$	$3\,^3D$
σ_P	0.5	2.2	17.2	24.0	0.2	7.6
σ_T	0.6	2.5	21.7	18.8	0.3	6.9

III. DISCUSSION

A. Structures observed on the excitation functions

Figure 4 shows the excitation functions of the He $3\,^1P$ level for target excitation by He^+, proton, and electron impacts, and for electron capture of the projectile by He^+ impacts [7–9] [the cross sections in the velocity range less than 5×10^6 m/s are the same as those in Fig. 2(c)]. On the excitation function of target He by He^+ impacts (σ_T), the largest structure T_d is observed in the velocity range larger than 2×10^6 m/s. It reaches its maximum value at about 5×10^6 m/s. We recognize similar

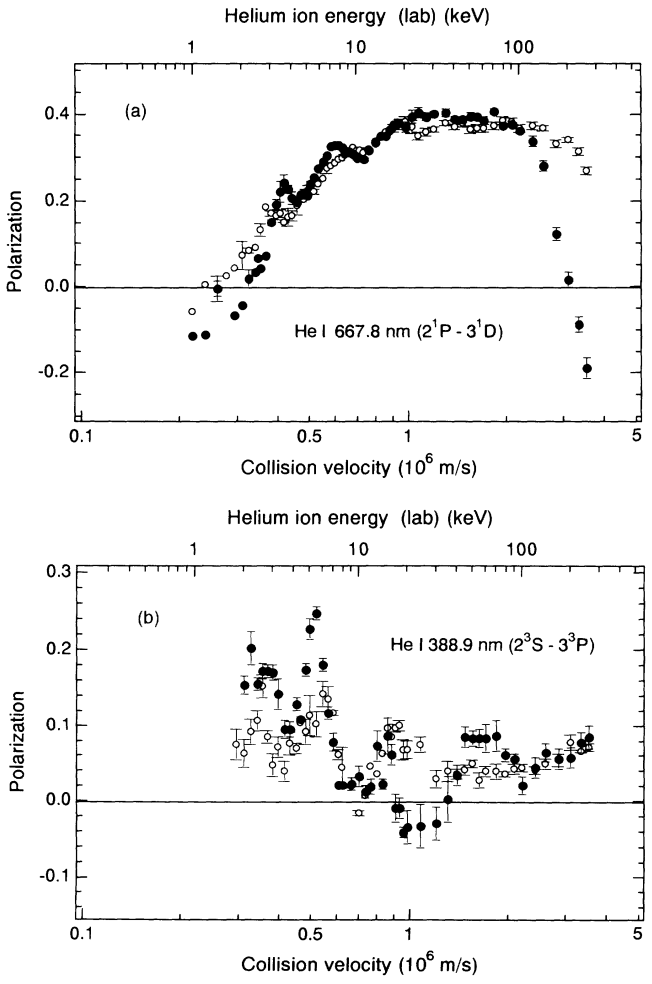

FIG. 3. Polarization degrees of emission from (a) $2\,^1P-3\,^1D$ and (b) $2\,^3S-3\,^3P$ transitions as functions of collision velocity in He^+-He collisions. Open circles, target excitation; solid circles, projectile excitation.

velocity dependence on the excitation functions generated by proton and electron impacts in nearly the same velocity range. This similarity indicates that these structures arise from $1\,^1S-3\,^1P$ dipole transition caused by the perturbative interactions in the high-velocity regime, which is rather insensitive to the constitutions of perturbing particles. A structure designated as T_{ex} follows the structure T_d in the velocity range from about $(1-2)\times10^6$ m/s.

The structure P_{cap} on the excitation function of electron capture (σ_P) into the $3\,^1P$ level arises in the velocity range from about $(1-4)\times10^6$ m/s in Fig. 4. The magnitude of σ_P of the $3\,^1P$ level is small in the velocity range larger than 3×10^6 m/s. The maximum value of P_{cap} is observed at the collision velocity larger than the velocity where the maximum of T_{ex} is observed.

It is well known that colliding particles form a quasimolecular state in the low-velocity regime. Electrons go around their classical molecular orbit many times during each interacting period. For the symmetric collision system of He^+-He, capture of electrons by the projectile nucleus and by the target nucleus may happen equally at the dissociation of the quasimolecular state. In fact, the magnitude of σ_P of the $3\,^1P$ level is nearly equal that of σ_T in the velocity range less than about 1×10^6 m/s in Fig. 4. Therefore we can regard this velocity range as the low-velocity regime for $3\,^1P$-level excitation.

In the low-velocity regime of He^+-He collisions, σ_T and σ_P show oscillations that are strong or weak, against impact velocity in antiphase with each other, which are interpreted being caused by the interference between the gerade and ungerade states of the helium quasimolecular ion [3].

On σ_T and σ_P of the $3\,^3P$ level in Fig. 2(d), we recognize the structures which seem to correspond to the structures observed in σ_T and σ_P of the $3\,^1P$ level, except the structure T_d originating from perturbative interaction in the high-velocity regime. Corresponding structures in Fig. 2(d) are designated by the same symbols used in Figs. 4 and 2(c). We find clear oscillations on σ_T and σ_P in antiphase with each other in the velocity range less than about 1×10^6 m/s. We define this velocity range as the low-velocity regime for the $3\,^3P$ level.

The profile of P_{cap} of the $3\,^3P$ level in Fig. 2(d) is affected by a steep rising at a velocity of about 2.2×10^6 m/s (x_2) owing to the overlapping of the 3867-Å line of the HeI $2\,^3P-6\,^3S$ transition in the spectroscopic measurement. The measured line intensity of the $2\,^3S-3\,^3P$ transition of helium atoms moving at a velocity of 2.2×10^6 m/s is $\frac{1}{17}$ that for rest particles [Eq. (6)].

The cross sections of the $3\,^3P$-level excitation by proton impact in Fig. 2(d) are small in the velocity range observed. This result coincides with the measurement in the low-velocity range by van Eck, de Heer, and Kistemaker [10]. The small magnitude of the triplet-level cross sections by structureless-particle impact means a small probability of spin flip by collision (according to the spin conservation rule of Wigner). Therefore the dominant process of the target triplet-level excitation is inevitably accompanied by exchange of the electrons with an-

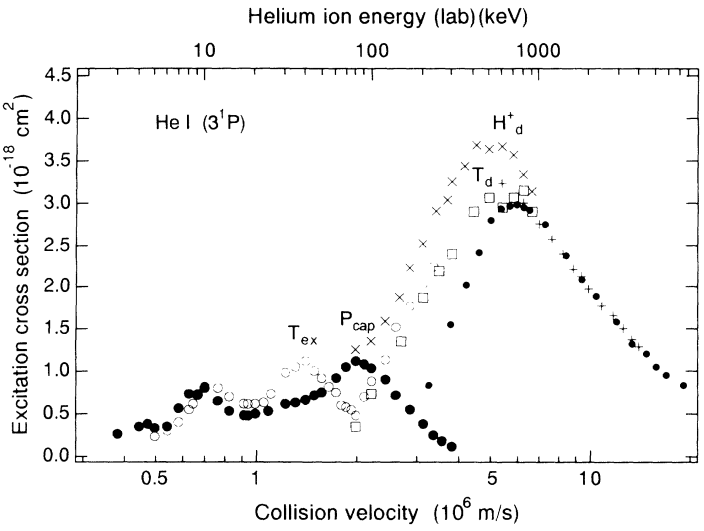

FIG. 4. Excitation functions of the He $3\,^1P$ level. Open circles and solid circles; present results for target and projectile excitation in He^+-He collisions, respectively; open squares, target excitation in He^+-He collisions from Ref. [7]; oblique crosses, present results for target excitation in H^+-He collisions; crosses, target excitation in H^+-He collisions from Ref. [8]; small solid circles, target excitation in e-He collisions from Ref. [9].

tiparallel spins. The small magnitude of σ_T of the $3\,^3P$ level in the velocity range higher than 3×10^6 m/s indicates that the probability of the excitation being accompanied by electron exchange is small in this velocity range.

The spin angular momentum does not couple with the electric field induced by a collision according to restrictions of the nonrelativistic theory. Then it is natural to consider that the excitation process accompanied by exchange of electrons with parallel spins scarcely contributes to excite the target $3\,^1P$ level in the velocity range larger than 3×10^6 m/s, in which neither the target $3\,^3P$-level excitation accompanied by exchange of electrons with opposite spins nor electron capture into the $3\,^1P$ level by projectile is significant. The relation between collision velocities to raise electron capture into the excited level and to raise the excitation accompanied by electron exchange is discussed in Sec. III B in detail.

The similar behaviors of the excitation functions by proton impact (structureless-particle impact) and by helium-ion impact in the high-velocity regime in Fig. 4 support the above inference. The behavior of the excitation function of electron impact is different from those of proton- and helium-ion impacts in the velocity range less than 5×10^6 m/s. This difference is explained as follows: the abscissa of collision velocity in the figure is nearly equal to $v_{\rm rel}$ for heavy-particle collisions in the velocity range observed. However, in electron-impact excitation, the velocity of an electron at the last stage of the interaction may be much different than the incident collision velocity, because most of the kinetic energy of the electron is consumed by excitation of the target. If the abscissa is rewritten in actual $v_{\rm rel}$, the excitation function by electron impact may extend into the low-velocity side.

The structure $T_{\rm ex}$ of the triplet level is generated by an actual exchange of electrons with antiparallel spins. On target singlet-level excitation, observation of the exchange of electrons with parallel spins is not possible because the electrons are indistinguishable. However, we expect that the same excitation mechanism that produces $T_{\rm ex}$ of the triplet-level cross section is effective in the production of the corresponding structure of singlet-level cross sections, and we use the same symbol $T_{\rm ex}$ to designate both structures (cf. Sec. III C).

The above discussion about the $3\,^{1,3}P$ level is applicable, on the whole, to $3\,^{1,3}S$ and $3\,^{1,3}D$ levels. For $3\,^1S$- and $3\,^1D$-level excitation, the structures in the high-velocity regime are attributed to quadrupole transitions caused by perturbative interaction. Then we designated the structures by the symbol T_q in Figs. 2(a) and 2(e), instead of T_d in Fig. 2(c). For $1\,^1S-3\,^1S$ quadrupole excitation in Fig. 2(a), the cross section by He^+ impact is smaller than that by H^+ impact, though the dependences of both cross sections on collision velocity resemble each other. Conversely, the cross section by He^+ impact is larger than that by H^+ impact for $1\,^1S-3\,^1D$ quadrupole excitation in Fig. 2(e). Since the interaction range of quadrupole excitation is much smaller than the range of dipole excitation, different constitutions of perturbing particles result in different magnitudes of cross sections for quadrupole transitions.

The structure $P_{\rm cap}$ on σ_P in Fig. 2(a) is affected by superposition of the structure X_1 of considerable magnitude, the origin of which we could not identify. The humps designated as T_x on σ_T in Figs. 2(e) and 2(f) look like the structures which correspond to $T_{\rm ex}$ in Fig. 4. However, the variation of σ_P (P_x) is in antiphase with respect to the variation of σ_T (T_x) in the corresponding velocity range. Then we conclude that T_x and P_x belong to the structures of the low-velocity regime. The low-velocity regimes extend up to about 1.3×10^6 m/s for $3\,^{1,3}D$-level excitation and we cannot find distinguishable structures that correspond to $T_{\rm ex}$ and $P_{\rm cap}$ (refer to Ref. [2] for details of structures in the low-velocity regime).

B. Characteristics of the structures in the intermediate-velocity regime

In this paper, the definition of velocity regimes is based on phenomenological behaviors of the excitation functions. There exist no clear boundaries between velocity regimes, because every excitation mechanism is possible

at all collision velocities. Our interest is in what excitation mechanism is dominant in the velocity regime. We consider that the boundary between the intermediate-velocity regime and the high-velocity regime on σ_T of the singlet level (a rough guess) exists near the dip between T_d or T_q and T_{ex}. The boundaries between the intermediate-velocity regimes and the high-velocity regimes on σ_P of singlet and triplet levels and on σ_T of the triplet level exist somewhere in the velocity ranges where the magnitudes of P_{cap} and T_{ex} become sufficiently small with an increase of collision velocity, respectively. The boundary between the intermediate- and low-velocity regimes is hypothesized as the range where σ_T and σ_P begin to oscillate in antiphase with each other. The boundaries on the different excited-level cross sections appear in different velocity ranges.

The characteristic velocity of an electron in the ground state of a helium atom is 3.3×10^6 m/s [11]. When the collision velocity is 1×10^6 m/s, the electron goes around the classical orbit of the ground state for the duration of the interaction, if the radius of the interaction range is the same as the radius of the orbital motion. The boundary between the high- and intermediate-velocity regimes assigned in the above discussion is in the range where v_{rel} is nearly equal to v_{elec} of the electron in the ground state. In most of the intermediate-velocity regime the electron does not complete its classical orbit for the duration of the interaction.

The processes of electron capture into an excited level and excitation accompanied by electron exchange seem by nature to be some kind of molecular process. The structure T_{ex} may seem to be the last cycle of the oscillation in the low-velocity regime. However, we do not find any antiphase oscillation on σ_P with respect to the variation of σ_T in the corresponding velocity range. Therefore the structures T_{ex} and, in addition, P_{cap} are distinguished from the structures in the low-velocity regime. We recognize characteristic relations between T_{ex} and P_{cap} that are common to most of the excited levels observed.

(1) The structure T_d or T_q, if it exists, is significant in the highest-velocity range, and P_{cap} and T_{ex} follow it. The velocities $v(T_d^{max})$ or $v(T_q^{max})$, $v(P_{cap}^{max})$, and $v(T_{ex}^{max})$ at which T_d or T_q, P_{cap}, and T_{ex} become maximum values, respectively, appear also in the same order:

$$v(T_{ex}^{max})<v(P_{cap}^{max})<v(T_q^{max}) \text{ or } v(T_d^{max}) . \quad (8)$$

The ratio $R=v(P_{cap}^{max})/v(T_{ex}^{max})$ is shown in Table III, in addition to $v(P_{cap}^{max})$ and $v(T_{ex}^{max})$ for $n=3$ and 4 levels. The relation below holds for most of the excited levels:

$$\frac{v(P_{cap}^{max})}{v(T_{ex}^{max})}\simeq 1.4 . \quad (9)$$

(2) Generally, the maximum value of T_{ex}, $\sigma_{max}(T_{ex})$, is smaller than the maximum value of P_{cap}, $\sigma_{max}(P_{cap})$:

$$\sigma_{max}(T_{ex})<\sigma_{max}(P_{cap}) . \quad (10)$$

(3) The polarization degrees of the emissions from the levels populated by the electron-capture process and by the electron-exchange process maintain nearly equal constant value through the intermediate-velocity regime, contrary to the significant change and oscillations in the low-velocity regime (Fig. 3). The rapid decrease of the velocity at about 2.2×10^6 m/s for the projectile $3\,^3P$-level in Fig. 3(b) is due to the overlap of the 3867-Å line of $P=0$.

When we consider T_{ex} or P_{cap} of the same spin multiplicity, it is possible to recognize the following characteristics of the dependence of magnitude and peak position on the angular-momentum state of the excited level.

(4) The peak of the S-level cross section is observed in the high-velocity side relative to the peak of the P-level cross section. The peaks of T_{ex} and P_{cap} of the D level are indistinguishable, because T_{ex} and P_{cap} of the D level are small in magnitude and may be located in low-velocity range in comparison with those of the S and P levels:

$$v(n\,^{1,3}D)\simeq v(n\,^{1,3}P)<v(n\,^{1,3}S) \text{ for } v(P_{cap}^{max}) , \quad (11)$$

$$v(n\,^{1,3}D)\simeq v(n\,^{1,3}P)<v(n\,^{1,3}S) \text{ for } v(T_{ex}^{max}) , \quad (12)$$

where $n=3$ and 4. This angular-momentum dependence of the peak positions was previously pointed out by de Heer and van den Bos [12]. The angular-momentum dependencies of Eqs. (11) and (12) are quite different from Eq. (13) below, which indicates the relation among peak positions of T_d and T_q in the high-velocity regime:

$$v(3\,^1D)\simeq v(3\,^1S)<v(3\,^1P) \text{ for } v(T_d^{max}) \text{ and } v(T_q^{max}) . \quad (13)$$

(5) The angular-momentum dependencies of magnitudes of T_{ex} and P_{cap} are described as follows:

$$\sigma(3\,^{1,3}D)<\sigma(3\,^{1,3}P)<\sigma(3^{1,3}S) \text{ for } \sigma_{max}(P_{cap}) , \quad (14)$$

$$\sigma(3\,^{1,3}D)<\sigma(3\,^{1,3}P)\lesssim\sigma(3\,^{1,3}S) \text{ for } \sigma_{max}(T_{ex}) . \quad (15)$$

The angular-momentum dependence of magnitude of

TABLE III. The velocities at the maxima of the excitation cross sections in the intermediate-velocity regime (10^6 m/sec) and ratio $R=v(P_{cap})/v(T_{ex})$.

	^1S			^1P			^1D			^3S			^3P			^3D		
n	$v(T_{ex}^{max})$	$v(P_{cap}^{max})$	R	$v(T_{ex}^{max})$	$v(P_{cap}^{max})$	R	$v(T_{ex}^{max})$	$v(P_{cap}^{max})$	R	$v(T_{ex}^{max})$	$v(P_{cap}^{max})$	R	$v(T_{ex}^{max})$	$v(P_{cap}^{max})$	R	$v(T_{ex}^{max})$	$v(P_{cap}^{max})$	R
3	1.5	2.2	1.5	1.4	2.0	1.4				1.8	2.5	1.4	1.6	2.2	1.4		(2.1)	
4	1.6[a]	2.1[b]	1.3	1.4[a]	2.0[b]	1.4	(1.2[a])	1.7[b]	(1.4)	1.8[a]	2.5[b]	1.4	1.6[a]					

[a]Reference [12].
[b]Reference [4].

the structure in the high-velocity regime is described as

$$\sigma(3\,^1D) < \sigma(3\,^1S) < \sigma(3\,^1P)$$
$$\text{for } \sigma_{\max}(T_d) \text{ and } \sigma_{\max}(T_q) . \quad (16)$$

In low-velocity collisions, S-level excitation by rotational coupling needs two-step molecular excitation, that is, $\Sigma \rightarrow \Pi \rightarrow \Sigma$, in the He^+-He collisions [2]. Consequently, S-level cross sections are small in comparison with other excited-level cross sections, as we find this tendency in the low-velocity regimes of Figs. 2(a) and 2(b). The considerable magnitude of the S-level cross section in the intermediate-velocity regime is worth noting.

C. Considerations about the excitation mechanism in the intermediate-velocity regime

It is interesting to examine whether the characteristics described in Sec. III B are unique to He^+-He collisions. Figures 5 and 6 show the cross sections of electron capture by H^+ into $H(3,l)$ in H^+-Li collisions [13] and H^+-He collisions [14,15] of near-symmetric systems, respectively. In both figures, we find the relation of Eq. (17) for the velocities at which maximum cross sections $\sigma_{\max}$ are observed:

$$v(3d) \simeq v(3p) < v(3s) \quad \text{for } v(\sigma_{\max}) . \quad (17)$$

Equation (17) is similar to Eq. (11) for $v(P_{\text{cap}}^{\max})$ in He^+-He collisions.

In Fig. 5 the magnitudes of s-level cross sections are comparable to those of p-level cross sections in most of the velocity range observed. In Fig. 6 we find the relation of Eq. (18) for $\sigma_{\max}$, which agrees with Eq. (14) for $\sigma_{\max}(P_{\text{cap}})$ in He^+-He collisions:

$$\sigma(3d) < \sigma(3p) < \sigma(3s) \quad \text{for } \sigma_{\max} . \quad (18)$$

It is noticeable that similar behavior of the cross sections have been observed on the above three collision systems. In all the excitation processes considered, s-level

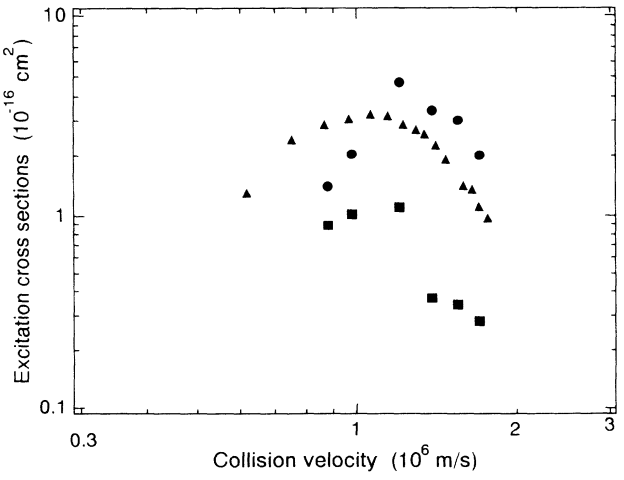

FIG. 5. Cross sections of electron capture into $H(3,l)$ levels in H^+-Li collisions. Solid circles, $3s$ level; solid triangles, $3p$ level; solid squares, $3d$ level from Ref. [13].

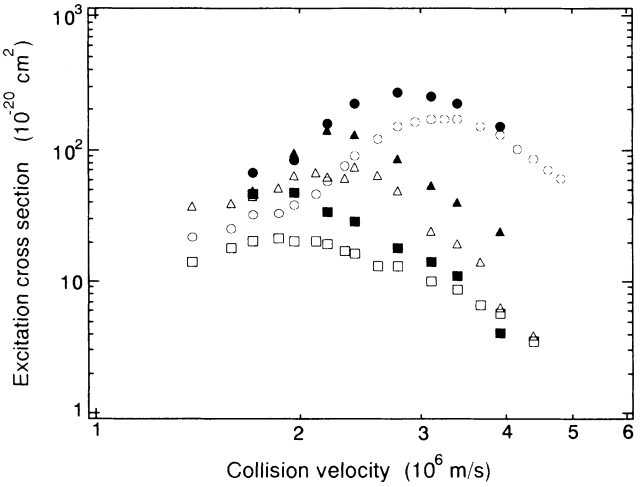

FIG. 6. Cross sections of electron capture into $H(3,l)$ levels in H^+-He collisions. Open circles, $3s$ level; open triangles, $3p$ level; open squares, $3d$ level from Ref. [14]. Solid circles, $3s$ level; solid triangles, $3p$ level; solid squares, $3d$ level from Ref. [15].

electrons are captured into upper s, p, and d levels. This fact suggests that the same kind of excitation mechanism is effective in the velocity ranges where the processes of electron capture into excited levels become significant and the behaviors of excitation functions closely correlate with the angular-momentum states of the initial and the final levels.

The methods to calculate cross sections of electron capture into excited levels in the intermediate-velocity range have been discussed in Ref. [16] and references therein. Processes of state-selective electron capture in atom–highly-charged-ion collisions were reviewed by Janev and Winter [17]. The close-coupling method is one of several powerful methods for describing the low- and intermediate-velocity collisions. The types of ETF (electron-translation factor) and switching functions are important factors to be determined in this method. The behaviors of the calculated results vary with selections of basis functions, types of ETF, and switching functions, in many cases. It is hard at present to say that the dependencies of the behaviors of the cross sections on angular-momentum states in the intermediate-velocity regime have been sufficiently explained.

One of the simple excitation models that reflects the characteristics of the angular-momentum states of the initial and final levels is the model in which the momentum of the captured electron is conserved through the electron-transfer process. In the Oppenheimer-Brinkmann-Kramers (OBK) approximation for high-velocity collisions, one of the important conditions for causing electron transfer is "momentum matching;" an electron jumps to the velocity-matching orbit without change of velocity. Bates and Dalgarno [18] calculated the cross sections of electron capture into $H(3,l)$ levels in H^+-H collisions by the OBK approximation, including the nuclear-interaction potential. The order of the peak positions of the $H(3,l)$-level cross sections obtained from their results is given by Eq. (19):

$$v(3s) < v(3p) \simeq v(3d) \quad \text{for } v(\sigma_{\max}) . \tag{19}$$

It shows a tendency that is the reverse of the order given by Eq. (17) and rather agrees with the order of the magnitudes of the root-mean-square averages of momenta $\mathbf{p}_{av}$ of H($3,l$) levels; the $\mathbf{p}_{av}$ of $3s$, $3p$, and $3d$ levels are 0.326, 0.332, and 0.333 in atomic units, respectively. The disagreement with the measured results arises from neglect of the higher-order terms in the first-order-perturbation methods, we think.

It is not easy to take into account the higher-order terms in the calculation. We calculated the overlapping integral of the initial- and final-state wave functions in momentum space, in order to examine the correlation between the characteristics observed and the momentum-matching process. In this simple model, momentum $\mathbf{p}$ of a target-atom electron is regarded as $\mathbf{p}-m_e\mathbf{V}$ (m_e; electron mass) by a projectile ion moving with velocity $\mathbf{V}$. A target-atom electron in the initial state $\psi_{\text{targ}}(\mathbf{p})$ is transferred into the final state of the neutralized projectile ion $\psi_{\text{proj}}(\mathbf{p}-m_e\mathbf{V})$. Then we define the transition probability P as

$$P = |\langle \psi_{\text{proj}}(\mathbf{p}-m_e\mathbf{V}) | \psi_{\text{targ}}(\mathbf{p}) \rangle|^2 , \tag{20}$$

where ψ is a wave function in momentum space. Figure 7 shows the probabilities P as functions of $\mathbf{V}$ in H^+-H collisions.

$$\vec{H}^+ + H \rightarrow \vec{H}(3,l) + H^+ . \tag{21}$$

Here an incident proton captures the $1s_0$ electron of the hydrogen atom and generates excited-state $\vec{H}$ $3s_0$, $3p_0$, or $3d_0$. The characters nlm correspond to principal, azimuthal, and magnetic quantum numbers, respectively. The quantum axis is in the direction of the beam injection. The angular momentum dependence of peak positions expressed by Eq. (17) is recognized in the behaviors of transition probabilities versus collision velocity in Fig. 7. The maximum value of the probability of the s-level cross section is much larger than that of the d-level cross section.

The transition probabilities of $1s_0$ to the $m_l \neq 0$ levels are quite small compared with those to the $m_l = 0$ levels all through the velocity range, owing to the property of $\Phi(\phi)$ functions [19]. The alignment of magnetic-sublevel populations results in polarization of emitted radiations. Unfortunately we have no data about the polarization of emission for the electron-capture process in the intermediate-velocity range of H^+-H collisions. The measurements for H^+-He collisions have proven the alignment of $m_l = 0$ levels in electron capture into H($3,l$) levels [20].

The qualitative agreements between the calculations of the momentum-matching model and the measurements

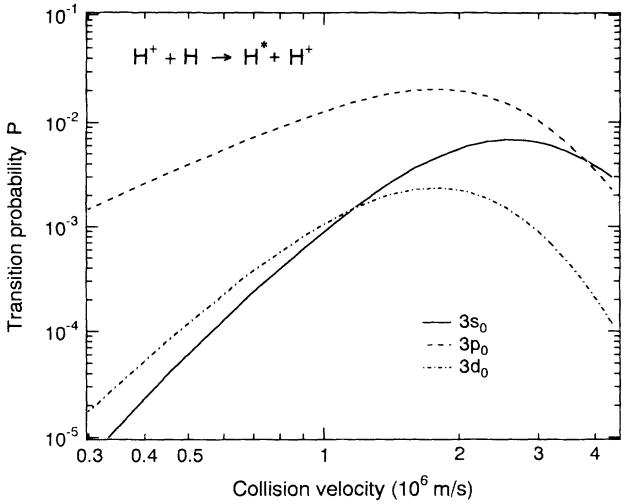

FIG. 7. Velocity dependences of transition probabilities (overlapping integral in momentum space) between H $1s_0$ and H $3s_0$ (solid line), $3p_0$ (broken line), and $3d_0$ (dashed and dotted line).

suggest that the electron is captured "directly" into the projectile excited-state orbit. This point is different from the excitation mechanism in the low-velocity collisions. According to the simplified method of the coupled-channel equations for low-velocity collisions [17], colliding particles form at the first stage the quasimolecular state of the lowest energy, and the dynamic coupling between quasimolecular states that is characterized by the magnitude of the coupling matrix element and the type of potential curve crossing gives rise to excitation of the quasimolecular state. Thus we have no reason to expect behaviors of cross sections regularly depending upon angular-momentum states in various collision systems.

If the radius of interaction range R_{int} is fixed for all collision velocities, $R_{\text{int}}/v_{\text{rel}}$ gives the duration of interaction. Equation (8) indicates that direct excitation by the perturbative interaction (no electron-transfer process) is attained with a small duration of the interaction. Electron capture into an excited level (single-electron-transfer process) needs finite interaction time. Equation (9) indicates that excitation accompanied by electron exchange (double-electron-transfer process) needs a duration about 1.4 times longer than that necessary for electron capture. On the other hand, we recognize similarities between Eqs. (11) and (12) and also between Eqs. (14) and (15). These similarities suggest that the same kind of excitation mechanism is effective in both processes of electron capture into the excited level and the excitation accompanied by electron exchange. Then we consider that the excitation accompanied by electron exchange consists of a two-step electron transfer:

$$\vec{He}(\uparrow)^+ + He(\uparrow\downarrow) \rightarrow \begin{cases} \vec{He}(\uparrow\downarrow\cdot\uparrow)He^+ \rightarrow \vec{He}(\uparrow)^+ + He(\uparrow\downarrow)^* & (22) \\ \vec{He}(\uparrow\uparrow\cdot\downarrow)He^+ \rightarrow \vec{He}(\uparrow)^+ + He(\uparrow\downarrow)^* & (23) \end{cases} \quad \text{for singlet}$$

$$\vec{He}(\uparrow)^+ + He(\uparrow\downarrow) \rightarrow \vec{He}(\uparrow\downarrow\cdot\uparrow)He^+ \rightarrow \vec{He}(\downarrow)^+ + He(\uparrow\uparrow)^* \quad \text{for triplet} . \tag{24}$$

Here the arrows pointing up and down indicate directions of electron spins, and symbols such as $\overrightarrow{He}(\uparrow\downarrow\cdot\uparrow)He^+$ indicate intermediate states in the electron-exchange process. We assume that the two electrons with equal spins in the intermediate state do not settle in the same state at the same time. First, incident ions capture electrons from target atoms (the one-electron capture cross section is a monotonically decreasing function of collision velocity in He^+-He collisions [21]). Electron capture into excited-state orbits occurs in a few cases. When the duration of the collisional interaction is sufficiently long, the electron transfer from neutralized ions to ionized targets follows and, in a few cases, the electrons are captured into the excited-state orbits of target atoms. As a consequence, the number of the events in which the excitation accompanied by electron exchange is possible is not so much smaller than the number of the events being able to cause electron capture into the excited level: this results in a smaller magnitude of the excitation cross section of electron exchange, but not so much smaller than the cross section of electron capture into the excited level [Eq. (10)].

Similar behaviors of polarization between the target and projectile cross sections in Figs. 3(a) and 3(b) also suggest that the excitation mechanisms for both processes are quite similar to each other in the intermediate-velocity regime. The polarization degrees of 0.04–0.08 for the $2\,^3S-3\,^3P$ transition [Fig. 3(b)] indicate that selective excitation to the $M_L=0$ magnetic sublevel [3] occurs all through the intermediate-velocity regime. Selective excitation to $M_L=0$ magnetic sublevels is consistent with the result derived from our excitation model. Constant polarization degrees [(5) in Sec. III B] show no drastic alteration of the relative population of the magnetic sublevel through the intermediate-velocity regime.

IV. CONCLUSION

On He^+-He symmetric collisions, the duration of collisional interaction plays an important role in determining the type of dominant process in the velocity range. In collisions of short duration in the high-velocity range, the electron-exchange process scarcely contributes to target-atom excitation. In collisions of longer duration in the intermediate-velocity range, electron capture into the excited level by the projectile ion (single-electron-transfer process) becomes significant. In collisions of a duration of about 1.4 times longer than that necessary for electron capture into the excited level, the excitation accompanied by electron exchange (double-electron-transfer process) contributes to target-atom excitation significantly. The boundary between the high- and intermediate-velocity regime exists in the range of the collision velocity that is nearly equal to the electron orbital velocity of the ground state. When the duration is so long as to be comparable to the period of classical orbital motion of the quasimolecular state formed during the collisional interaction, molecular excitation in the low-velocity collisions becomes dominant.

In much of the intermediate-velocity range, the transferred electrons do not complete classical orbits around the nuclei before dissociation of the quasimolecular states. What is the conserved quantity in these situations? Born approximation shows that momentum matching is an important condition in giving rise to electron capture in the high-velocity collisions. Our simple calculations of overlapping of wave functions in momentum space suggest the possible role of momentum matching in both the process of electron capture into the excited level and the process of excitation accompanied by electron exchange in the intermediate-velocity collisions.

[1] It may be unusual to use the word "excitation function" to describe velocity dependences of cross sections for electron capture and electron-exchange processes. However, we let cross sections for both processes be excitation functions, for convenience.
[2] R. Okasaka, Y. Konishi, Y. Sato, and K. Fukuda, J. Phys. B **20**, 3771 (1987).
[3] M. Tani, A. Hishikawa, and R. Okasaka, J. Phys. B **24**, 1359 (1991).
[4] L. Wolterbeek Muller and F. J. de Heer, Physica **48**, 345 (1970).
[5] K. Blum, *Density Matrix Theory and Applications* (Plenum, New York, 1981).
[6] A. Hishikawa, H. Mizuno, M. Tani, and R. Okasaka, J. Phys. B **25**, 3419 (1992).
[7] D. Hasselkamp, R. Hippler, A. Scharmann, and K.-H. Schartner, Z. Phys. **257**, 43 (1972).
[8] R. Hippler and K.-H. Schartner, J. Phys. B **7**, 618 (1974).
[9] F. G. Donaldson, M. A. Hender, and J. W. McConkey, J. Phys. B **5**, 1192 (1972).
[10] J. van Eck, F. J. de Heer, and J. Kistemaker, Physica **30**, 1171 (1964).
[11] K. R. Sandhya Devi and J. D. Garcia, J. Phys. B **16**, 2837 (1983).
[12] F. J. de Heer and J. van den Bos, Physica **31**, 365 (1965).
[13] F. Aumayr, M. Fehringer, and H. Winter, J. Phys. B **17**, 4201 (1984).
[14] R. H. Hughes, C. A. Stiger, B. M. Doughty, and E. D. Stokes, Phys. Rev. A **1**, 1424 (1970).
[15] J. Lenormand, J. Phys. (Paris) **37**, 699 (1976).
[16] B. H. Bransden and M. R. C. McDowell, *Charge Exchange and the Theory of Ion-Atom Collisions* (Clarendon, Oxford, 1992).
[17] R. K. Janev and H. Winter, Phys. Rep. **117**, 265 (1985).
[18] D. R. Bates and A. Dalgarno, Proc. Phys. Soc., London, Sect. A **66**, 972 (1953).
[19] B. Podolsky and L. Pauling, Phys. Rev. **34**, 109 (1929).
[20] J. R. Ashburn, R. A. Cline, P. J. M. van der Burgt, W. B. Westerveld, and J. S. Risley, Phys. Rev. A **41**, 2407 (1990).
[21] F. J. de Heer, J. Schutten, and H. Moustafa, Physica **32**, 1793 (1966); P. Mahadevan and G. D. Magnuson, Phys. Rev. **171**, 103 (1968); H. B. Gilbody, K. F. Dunn, R. Browning, and C. J. Latimer, J. Phys. B **4**, 800 (1971).